



Deposited via The University of Leeds.

White Rose Research Online URL for this paper:

<https://eprints.whiterose.ac.uk/id/eprint/184369/>

Version: Accepted Version

Article:

Roach, L, Coletta, PL, Critchley, K et al. (2022) Controlling the Optical Properties of Gold Nanorods in One-Pot Syntheses. *The Journal of Physical Chemistry C*, 126 (6). pp. 3235-3243. ISSN: 1932-7447

<https://doi.org/10.1021/acs.jpcc.1c10447>

© 2022 American Chemical Society. This is an author produced version of an article published in *Journal of Physical Chemistry C*. Uploaded in accordance with the publisher's self-archiving policy.

Reuse

Items deposited in White Rose Research Online are protected by copyright, with all rights reserved unless indicated otherwise. They may be downloaded and/or printed for private study, or other acts as permitted by national copyright laws. The publisher or other rights holders may allow further reproduction and re-use of the full text version. This is indicated by the licence information on the White Rose Research Online record for the item.

Takedown

If you consider content in White Rose Research Online to be in breach of UK law, please notify us by emailing eprints@whiterose.ac.uk including the URL of the record and the reason for the withdrawal request.

Controlling the Optical Properties of Gold Nanorods in One-Pot Syntheses

Lucien Roach^{1†}, P Louise Coletta², Kevin Critchley¹, and Stephen D. Evans^{1}*

1. School of Physics and Astronomy, University of Leeds, Leeds, LS2 9JT, UK
2. Leeds Institute for Medical Research, University of Leeds, Leeds, LS2 9JT, UK

Keywords: gold nanorods, binary surfactants, kinetics, synthesis, one-pot

Abstract: We present the characterization of the CTAB-oleate controlled synthesis of gold nanorods (AuNRs). Concentrations of key compounds in the synthetic system were varied in the presence of oleate; including HCl, borohydride, silver nitrate, ascorbic acid. The longitudinal surface plasmon resonance peak was sensitive to changes in all concentrations. Reducing the concentration of Ag ions below 66 μM led to slower reaction kinetics and incomplete Au reduction. Variation of ascorbic acid concentration revealed that oleate is responsible for around 44% of the reduction of Au^{3+} to Au^{1+} before nucleation in these experiments. Increasing the oleate concentration significantly slows the growth kinetics and leads to much longer synthesis times above 12 h for reaction completion. These observations will enable the design of better syntheses of AuNR utilizing binary surfactants.

1. Introduction.

Gold nanorods (AuNRs) are one of the most heavily researched gold nanoparticle morphologies.¹⁻⁴ AuNRs have narrow extinction peaks tunable throughout red and near-infrared through control of their aspect ratio and their dielectric environment.⁵ They also offer the largest plasmonic response per unit mass of Au of all gold nanoparticles, capable of strong field enhancement at their tips and efficient conversion of light-to-heat.⁶⁻⁸ This combination of properties has meant that they have found application in roles such as optical sensors,⁹ surface-enhanced Raman spectroscopy probes,¹⁰ and photothermal conversion agents in photothermal therapy and photoacoustic imaging.^{1,11} Thus, there is considerable interest in the synthesis of AuNRs and controlling their optical properties.

Jana *et al.* published the first seeded AuNR synthesis in 2001, which reduced a gold salt onto pre-synthesized Au seeds in a cetyltrimethylammonium bromide (CTAB) solution using ascorbic acid (AA).¹¹ This protocol has since seen many modifications, of note are the inclusion of silver ions¹² and the optimization of reaction pH,¹⁴ which both resulted in an improved yield of rod-like nanoparticles. The inclusion of silver salts also notably resulted in the production of monocrystalline AuNRs (as opposed to pentatwinned AuNRs). More recent innovations have focused on the inclusion of additives in the growth solution to further improve the yield and monodispersity of the synthesized AuNRs. These have broadly consisted of (1) aromatic molecules, such as salicylate,^{15,16} dopamine,¹⁷ hydroquinone,¹⁸ or resveratrol;¹⁹ (2) co-surfactants like benzyldimethylhexadecylammonium chloride^{13,20} and oleate;²¹⁻²⁴ or (3) Hoffmeister salts.²⁵ As well as replacing CTAB with alternative surfactants such as dodecylethyldimethylammonium bromide²⁶ or Gemini surfactants.²⁷ These improvements have made AuNR syntheses more reliable, improved the quality of the end-products, and provided additional means to control the

optical properties (and hence morphology) of synthesized AuNRs. AuNRs can also be synthesized through the direct reduction of the HAuCl_4 in the growth solution using a strong reducing agent such as NaBH_4 without the presence of seeds in ‘one-pot’ (or ‘seedless’) protocols which can also produce monodisperse AuNRs in high purity.

However, there remains debate around the exact processes that occur during the AuNR syntheses and the role of each component. For instance, the mechanism by which Ag ions function as a facet-specific capping agent is still debated. Both the underpotential deposition of a Ag^0 monolayer,^{28–31} and the formation of surface-bound CTA-Ag-Br,^{28,32} have been suggested. Currently, the opinion in the literature mostly favors the former, but it has not been conclusively proven as the mechanism. There is also still debate around the role of the reducing agent ascorbic acid. Some researchers suggest that AuNR growth occurs through an autocatalytic disproportionation reaction ($3\text{Au}^{1+} \rightarrow 2\text{Au}^0 + \text{Au}^{3+}$) with the ascorbic acid reducing the produced Au^{3+} ions back to Au^{1+} to continue the reaction.³³ Whereas others have suggested that it directly reduces Au^{1+} onto the surface of the AuNR.³⁴ The latter has become more widely accepted following reports that no particle growth occurs when ascorbic acid is replaced with weaker reducing agents, such as salicylate and oleate. These can reduce Au^{3+} to Au^{1+} , but not Au^{1+} to Au^0 , meaning that these cannot drive particle growth in the absence of a disproportionation reaction, and hence direct reduction is more likely as the growth mechanism.^{15,21}

We previously reported that the aspect ratio of AuNRs was tunable through variation of the surfactant concentrations used in a ‘one-pot’ binary surfactant-based protocol.²² The inclusion of a second surfactant, sodium oleate, improves the monodispersity and shape yield of the synthesized nanorods.^{21,22} However, the introduction of oleate alters the properties of the reaction medium and changes the reactant concentrations required for AuNR growth. Here we report the effects of

changing the concentrations of HCl, borohydride, silver nitrate, and ascorbic acid on AuNR syntheses in the presence of oleate. We also have investigated the effect of oleate on the kinetics of the synthesis.

2. Methods

2.1. Materials. L-ascorbic acid (AA, A15613) was purchased from Alfa Aesar. Hydrochloric acid (A144S-500), silver nitrate (11414), and sodium borohydride (10599010) were purchased from Fisher Scientific. Gold (III) chloride trihydrate (520918) and cetyltrimethylammonium bromide (CTAB, H6269) were purchased from Sigma-Aldrich. Sodium oleate (O0057) was purchased from TCI. All solutions were prepared using Milli-Q grade deionized water (18 M Ω ·cm).

2.2. Synthesis of gold nanorods. AuNRs were synthesized following our previously reported protocol.²³ AuNRs were prepared in 10 mL batches. The volumes and concentrations were varied as part of this study, but in a typical synthesis, solutions of CTAB and sodium oleate (200 mM) were prepared in advance, by heating to 70°C under stirring until all solute was dissolved. The solutions were cooled to 30°C before use. Vials were cleaned with *aqua regia* and thoroughly rinsed, before 2.4 mL CTAB, 0.625 mL oleate, and 1.925 mL water were added and mixed. This was followed by the sequential addition 5 mL HAuCl₄ (1 mM), 240 μ L AgNO₃ (4 mM), 50 μ L HCl (11.8 M), and 75 μ L ascorbic acid (85.8 mM). To this 7.5 μ L freshly prepared, ice-cold NaBH₄ (10 mM) was rapidly injected into the mixture. The mixture was then held at 30°C for 4 h. The AuNRs were isolated by centrifugation at 9000g for 30 min. The supernatant was discarded, and the precipitate resuspended in water. AuNR solutions were stored in the dark at room temperature. The concentrations given here are examples, any deviations from this protocol are

stated in the main text. All concentrations are given as the concentration in the total volume of the growth solution after the addition of all solutions (i.e. 2.4 mL 200 mM CTAB in a 10.4 mL growth solution yields $[CTAB] = 46.3$ mM).

2.3. UV-Vis spectrometry. For individual spectra, measurements were taken using an Agilent Cary 5000 UV-Vis-NIR using quartz cuvettes ($L_{\text{path}} = 1$ cm). Samples were typically diluted by a factor of 10 before spectra acquisition. Where spectra are presented un-normalized, they have been multiplied by the dilution factor to account for this (following the Beer-Lambert law).

For kinetic spectra, AuNR growth solutions were prepared as described above in a 10 mL vial, after the addition of the NaBH_4 the solution was mixed quickly and 700 μL pipetted into quartz cuvette ($L_{\text{path}} = 2$ mm) and the capture of spectra immediately started. Cuvettes were cleaned with *aqua regia* and rinsed thoroughly before use. During the first 5 h spectra were taken at 2 min intervals at $1800 \text{ nm}\cdot\text{min}^{-1}$. For the following 24 h spectra were taken at 10 min intervals at $900 \text{ nm}\cdot\text{min}^{-1}$. Solutions were maintained to 30°C throughout spectra acquisition. To account for the reduced path length spectra from these measurements are multiplied by a factor of 5 to retrieve the true extinction value (again following the Beer-Lambert law).

Where concentrations have been calculated from the extinction at 400 nm ($A_{400\text{nm}}$) this was done using the approximation $[\text{Au}^0] = c \cdot A_{400\text{nm}}$ (where $c = 0.42$ mM) given elsewhere in the literature.³⁵⁻
³⁷ This was confirmed experimentally using a Varian 240fs atomic absorbance spectrometer (Figure S1). In syntheses, which vary the concentration of Ag ions, the presence of Ag^0 is expected to have very little impact on $A_{400\text{nm}}$, because intraband transitions occur below this wavelength for Ag.⁵

2.3. Electron Microscopy. TEM images were obtained using a Tecnai G2 Spirit TWIN/BioTWIN with an acceleration voltage of 120 kV. TEM samples were prepared by drying ~5 μL of $10\times$ concentrated nanoparticle dispersion on an amorphous carbon-coated 400-mesh copper grid (Electron Microscopy Services, CF400-Cu).

3. Results

In a typical monocrystalline AuNR synthesis, a growth solution is prepared containing shape directing surfactants (in this case CTAB and oleate), a gold salt, and a silver salt (typically ~5:1 Au:Ag molar ratio). A small volume of HCl is then added to this, followed by a mild reducing agent, such as ascorbic acid. HCl is included to lower the pH to prevent ascorbic acid nucleating gold particles. Finally, either a thermally aged seed solution is added, or a small volume of NaBH_4 solution, a strong reducing agent which induces the nucleation of gold nanoparticles, is added. Further Au reduction then occurs onto these seeds with the surfactants and silver causing anisotropic growth. This study focuses solely on a ‘one-pot’ synthesis protocol using NaBH_4 .

The effects of the concentrations of HCl, AgNO_3 , ascorbic acid, and NaBH_4 in the growth solution are interrelated, making it difficult to categorically identify changes as the result of a single variable. However, the impact of the introduction of oleate on the other components was not well understood, hence we performed studies on each of these in the presence of oleate. Each component is discussed in the order in which they are added to the growth solution.

3.1. Effect of silver nitrate concentration. The presence of silver ions is essential to the formation of single-crystalline AuNRs. Silver plays two key roles in the formation process, it is critical to the initial symmetry breaking in the formation of nascent nanorods, and beyond this it is crucial

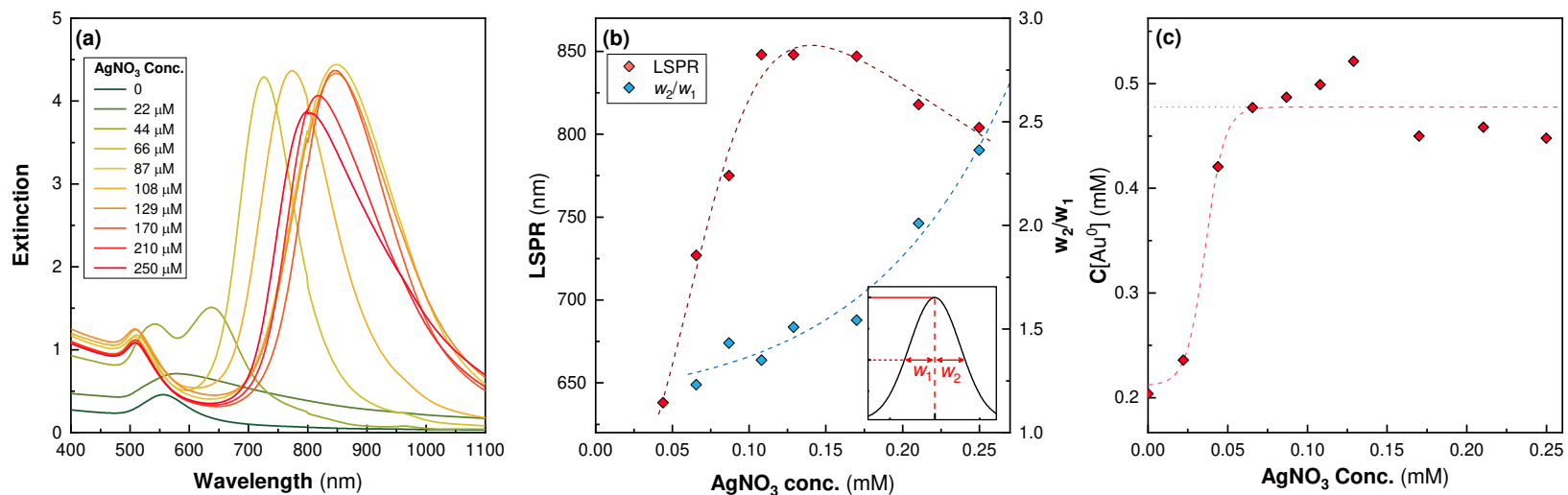


Figure 1. Effect of varying $[\text{Ag}]$ on AuNR spectra ($[\text{CTAB}] = 48 \text{ mM}$, $[\text{oleate}] = 15 \text{ mM}$) after 4 h. **(a)** UV-Vis spectra at different values of $[\text{Ag}]$. **(b)** λ_{LSPR} as a function of $[\text{Ag}]$. Also plotted is w_2/w_1 which is the ratio of the widths at half maximum above and below λ_{LSPR} (see inset). **(c)** $A_{400\text{nm}}$ after reaction completion. Results are fitted with a sigmoid. **[double column]**

to regulating the growth on the $\{110\}$ facets along the sides of AuNR through a cycle of galvanic replacement and silver deposition leading to continued anisotropic growth.^{29,30} Variation of $[Ag]$ in the growth solution should thus have a strong effect on the aspect ratio of synthesized nanorods.

We investigated the impact of the presence of Ag ions by varying $[Ag]$ between 0 and 250 μM in a growth solution containing $[CTAB] = 48 \text{ mM}$ and $[oleate] = 15 \text{ mM}$. UV-Vis spectra of AuNRs synthesized under these conditions are shown in Figure 1(a). In the absence of AgNO_3 , we observe only a single peak with a maximum at $\sim 560 \text{ nm}$, indicating that only gold nanospheres are present as seen in other reports in the literature.²⁹ At $[Ag] = 22 \text{ }\mu\text{M}$ we observe a single peak with a maximum at $\sim 580 \text{ nm}$ with a tail extending out into the near-infrared, suggesting a population dominated by nanospheres, but containing some anisotropic gold nanoparticles. There then appears to be a threshold, between 22 and 44 μM (Au:Ag = 22.7 and 11.4 respectively), above which a second well-defined peak in the near-infrared becomes apparent consistent with a longitudinal surface plasmonic resonance (LSPR). Combined with the lack of any peak at $\sim 560 \text{ nm}$ associated with non-rodlike side-products it seems that above this threshold the Au is near-completely in the form of AuNRs. Figure 1(b) shows that the maxima of the LSPR peak (λ_{LSPR}) increases with $[Ag]$ until it reaches a maximum value of $\sim 890 \text{ nm}$ at $[Ag] = 108 \text{ }\mu\text{M}$ (Au:Ag = 4.6). This shows that the raising $[Ag]$ increases the aspect ratio of the AuNRs. This trend has been widely observed elsewhere in the literature (e.g. refs. 13,14,18,30,38–42). Once $[Ag]$ is increased above $\sim 108 \text{ }\mu\text{M}$, λ_{LSPR} decreases and the longitudinal surface plasmon resonance peak becomes increasingly asymmetric as indicated by the increase in the ratio of upper half-width maximum to lower half-width maximum (w_2/w_1). This ratio is an indirect measure of the polydispersity resulting from increasingly large populations of higher aspect ratio AuNRs (Figure 1(b)). It was not possible to fit peaks where the transverse surface plasmon resonance (TSPR) and longitudinal surface

plasmon resonance peaks overlapped significantly, hence only the data for $[Ag] \geq 66 \mu\text{M}$ (Au:Ag = 7.6) is presented. The longitudinal surface plasmon resonance peak becomes increasingly shifted towards longer wavelengths. This is observable in the spectra of other publications, although normally it is not commented upon (i.e. ref. 43). It presumably results from the $\{110\}$ stabilizing role played by AgNO_3 which makes the formation of higher aspect ratio AuNRs more preferable, however, the limitations of this growth system seem to prevent these from forming with high uniformity.

The spectra of samples containing $[Ag] < 66 \mu\text{M}$ show an incomplete reduction of the gold salt after 4 h, and these spectra continued to evolve over the following 24 h (Figure S2). Thus, the growth kinetics of the AuNRs were slowed at lower $[Ag]$. There were no further changes in these spectra after an additional 24 h. It also seems that Ag is acting as a limiting reagent in this system. The final $A_{400\text{nm}}$ values indicate that there is a noticeable reduction in the fraction of ionic Au that was completely reduced at these lower concentrations (Figure 1(c)). Ag is thus acting as a limiting agent, which is a surprising result as Ag does not function as a reducing agent in this system and is only expected to affect the geometry of the particles. To our knowledge, both these observations have not been previously reported in the literature. Most reports suggest that the fraction of reduced Au is either independent of $[Ag]$,^{39,40} or increases with decreasing $[Ag]$.^{13,38,42} It is apparent based on these measurements is that $[Ag]$ between $\sim 44 \mu\text{M}$ and $\sim 170 \mu\text{M}$ is a reliable parameter to control λ_{LSPR} . Above this range, the polydispersity rapidly increases as an increasingly large population of higher aspect AuNRs form.

3.2. Effect of hydrochloric acid concentration. HCl is primarily included in the growth mixture to control the reaction pH. The redox potential of the mild reducing agent, ascorbic acid, is pH-

sensitive and thus the pH must be lowered to a value at which ascorbic acid cannot nucleate AuNPs but can reduce Au onto the surface of the nascent AuNRs post-NaBH₄ addition. Additionally, it also slows the reaction kinetics allowing more homogenous formation of AuNRs. For CTAB-only growth protocols typically a value of [HCl] around 14 mM (pH ~1.5) is required to prevent Au⁰ nucleation upon ascorbic acid addition.¹⁴ In our system the inclusion of the second surfactant, sodium oleate, makes the growth mixture more basic (solutions of sodium oleate above its critical micelle concentration typically have a pH of ~9.8).⁴⁴ Thus, the inclusion of oleate decreases the reduction potential and increases the reaction kinetics.⁴⁵⁻⁴⁷ The concentration of HCl added to the solution must be increased accordingly to prevent ascorbic acid-derived nucleation and to control the reaction kinetics. In the case of an oleate – CTAB mixture, we reported previously that [HCl] ~ 60 mM was required to produce the same result.²³

Hence the effect of changing [HCl] was explored by preparing a single growth solution containing [CTAB] = 48 mM, [oleate] = 12.5 mM, and [Au] = 0.5 mM . This was then aliquoted into 11 separate 10 mL batches, in which [HCl] was varied between 23 and 74 mM, followed by the two reducing agents. The spectra of the synthesized AuNRs and the respective LSPR positions are shown in Figure 2.

In the UV-Vis spectra, increasing [HCl] above 28 mM leads to high yields of AuNRs evident from relatively low absorbance around 520 nm. Increasing [HCl] leads to a redshift in λ_{LSPR} . The changes in the height of the peak are in line with what is expected from Gans' solution, due to decreased plasmonic damping by interband transitions above 600 nm, suggesting a high rod yield. The redshift in this peak appears to stop once [HCl] is increased above 54 mM (Figure 2(b)). HCl thus offers a method to fine-tune the λ_{LSPR} of synthesized AuNRs. The asymmetry in the

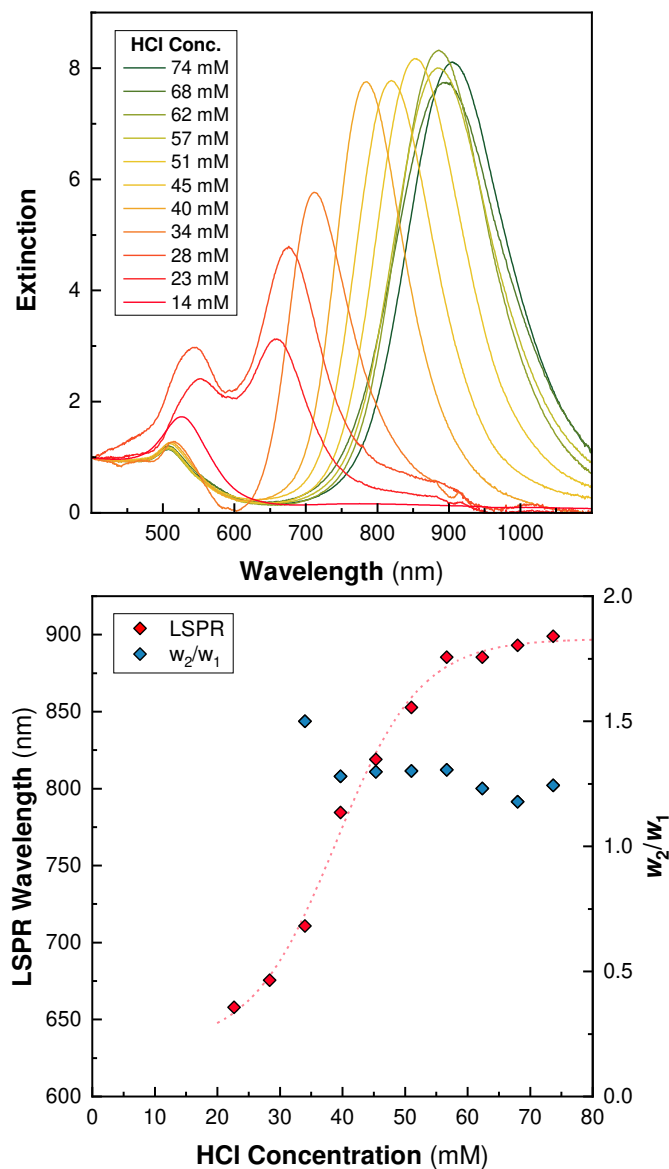


Figure 2. Effect of varying $[HCl]$ on AuNR spectra ($[CTAB] = 48 \text{ mM}$, $[Oleate] = 12.5 \text{ mM}$) **(a)** UV-Vis spectra normalised to $A_{400\text{nm}}$. Low $[HCl]$ ($\lesssim 30 \text{ mM}$) leads to high AuNS populations, increasing $[HCl]$ further leads to a redshift in λ_{LSPR} up to around $[HCl] \sim 58.5 \text{ mM}$. **(b)** λ_{LSPR} as a function of $[HCl]$, demonstrating the increase in λ_{LSPR} with increasing $[HCl]$. This behavior begins to plateau above $[HCl] \sim 59 \text{ mM}$. Also plotted is w_2/w_1 for spectra with longitudinal surface plasmon resonance peak (LSPR) well separated from the transverse peak. The data point associated with $[HCl] = 28 \text{ mM}$ has been omitted as no longitudinal surface plasmon resonance peak was visible. **[single column]**

longitudinal surface plasmon resonance peak measured by w_2/w_1 remains approximately constant around 1.25 above $[HCl] = 34$ mM suggesting that the polydispersity is not affected significantly by the concentration of $[HCl]$ above this value. For all subsequent syntheses, $[HCl] = 57$ mM was used. It is worth noting that variations in pH will still occur for other surfactant compositions due to the limited buffering capacity of the growth solution.

3.3. Effect of ascorbic acid concentration. Ascorbic acid (AA) is the primary reduction agent during the synthesis and changes in its concentration directly affect the kinetics of AuNR formation. In the binary surfactant system used here, the presence of oleate complicates matters. Oleate is a mild reducing agent, present at a higher concentration than ascorbic acid and at 30°C can reduce Au^{3+} to Au^{1+} . At higher temperatures ($\geq 50^\circ C$) the oleate – CTAB mixture alone can nucleate particles (i.e. without HCl, ascorbic acid, or $NaBH_4$).

To investigate the effects of ascorbic acid in this synthesis a single growth solution, containing $[CTAB] = 48$ mM and $[oleate] = 15$ mM, was split into several 10 mL batches following the same protocol as above and $[AA]$ was varied between 0 and 1.63 mM. The resulting spectra and change in longitudinal surface plasmon resonance are given in Figures 3(a) and (b) respectively. λ_{LSPR} increased linearly with increasing $[AA]$ up to ~ 1.43 mM, where this trend began to plateau. The synthesized rods had narrow symmetric peaks, as demonstrated by the relatively consistent w_2/w_1 values around ~ 1.25 (Figure 3(b)). All spectra had high $A_{LSPR}:A_{TSPR}$ ratios, with no evidence of non-rodlike nanoparticles. The reaction did not progress at all in the absence of ascorbic acid, consistent with oleate being incapable of reducing the Au^{1+} onto the particles under these reaction conditions.²¹ Values of $[AA] < 0.62$ mM incompletely reduce the Au salt, 4 h after the addition of $NaBH_4$. Further incubating at 30°C for an additional 24 h ($t_{total} = 28$ h) demonstrated that this

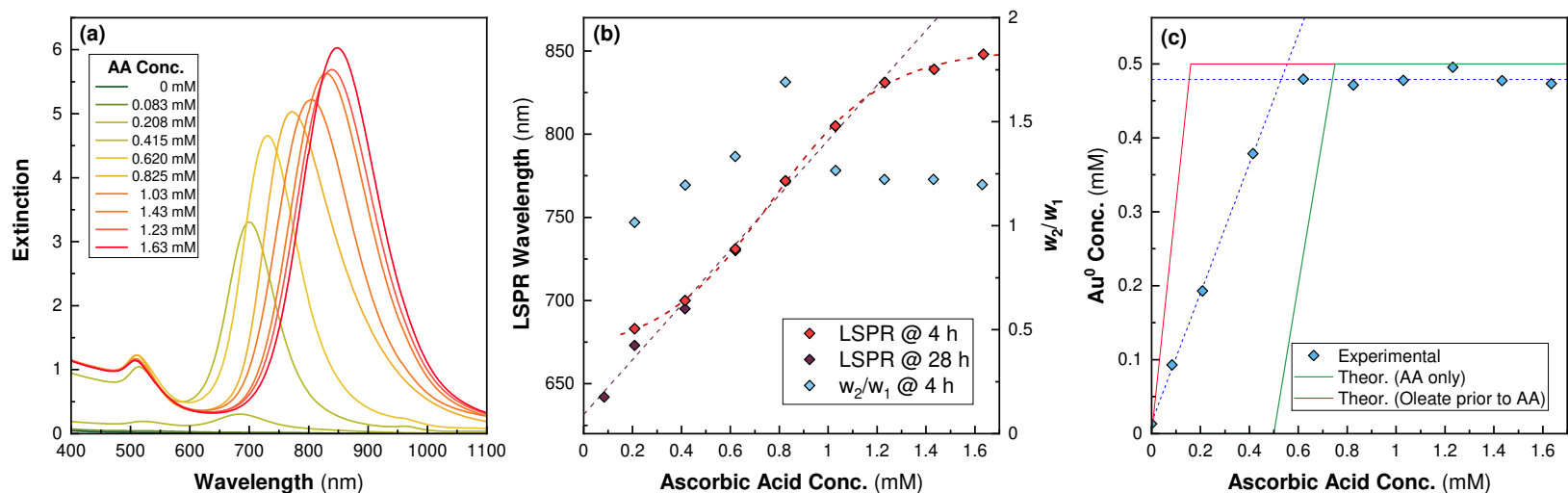


Figure 3. Effect of varying ascorbic acid concentration, $[AA]$, on AuNR spectra ($[CTAB] = 48 \text{ mM}$, $[oleate] = 15 \text{ mM}$) (a) UV-Vis spectra of AuNRs synthesized using different values of $[AA]$ 4 h after addition of NaBH_4 . Longitudinal surface plasmon resonance peaks (LSPR) were not visible for the 0 and 0.083 mM samples. The 0.21 and 0.42 mM samples did not completely reduce all Au^{3+} in solution based on $A_{400\text{nm}}$ (b) λ_{LSPR} as a function of $[AA]$. The values at 4 and 28 h after NaBH_4 addition are presented as separate series. A general trend of increasingly redshifted λ_{LSPR} can be seen with increasing $[AA]$. The values at 4 h are fitted with a sigmoid, the values at 28 h $[AA] < 1.43 \text{ mM}$ show a linear trend. Also plotted is w_2/w_1 for spectra with a longitudinal surface plasmon resonance peak which is well separated from the transverse peak. (c) $A_{400\text{nm}}$ after 28 h. The theoretical yield assuming perfect reduction Au^{3+} only by ascorbic acid is also plotted in green and assuming a complete reduction of Au^{3+} to Au^{1+} by oleate before ascorbic acid addition. **[double column]**

resulted from ascorbic acid acting as a limiting reagent below 0.62 mM. However, the spectra of samples with lower concentrations continued to evolve after 4 h, due to the slower reaction kinetics associated with lower $[AA]$ (Figure S3). This is most clear in the case of $[AA] = 83 \mu\text{M}$, where two previously undetectable peaks emerged in the spectrum after 28 h. For $[AA] = 208 \mu\text{M}$, there was a large increase in extinction at all wavelengths in the same period, suggesting that most of the Au^{1+} in solution was reduced during this time. All reactions appear to have been completed after 28 h and no further changes in the spectrum were observed after this point.

As shown in Figure 3(c), the near-complete reduction is observed ($>96\%$) for all samples above $[AA] \gtrsim 0.5 \text{ mM}$. Below this not all the gold salt is reduced to Au^0 , suggesting that ascorbic acid is the limiting reagent for $[AA] \lesssim 0.5 \text{ mM}$. The stoichiometric ratio of $\text{Au}^{3+}:\text{AA}$ for complete reduction to Au^0 is 1.5 without the presence of other reductants (i.e. $[AA] = 0.75 \text{ mM}$),⁴⁰ hence not all the reduction in this system is being caused by ascorbic acid. This can be seen from the way our data deviates from the theoretically expected curves for ascorbic acid acting as the sole reducing agent in Figure 3(c). Oleate thus appears to facilitate some reduction of the Au^{3+} to Au^{1+} . This reduction is partially provided by the ascorbic acid, as the observed yields also do not match that expected for a synthesis where all reduction of Au^{3+} to Au^{1+} is performed by oleate either. At the intersection of the two linear fits ($[AA] = 0.53 \text{ mM}$, i.e. where complete reduction to Au^0 should occur) would require $\sim 44\%$ reduction of Au^{3+} to Au^{1+} by oleate. The percentage of reduction done by oleate will increase with decreasing $[AA]$. This fraction is dependent on the time elapsed between the mixing of oleate and Au^{3+} , and the later addition of ascorbic acid, similar results have been reported for reduction with salicylic acid.¹⁵ Allowing more time to elapse should result in further reduction by oleate since it exists in a $30\times$ molar excess relative to Au. This may be desirable as it would increase the reproducibility of this synthesis by minimizing variation in the

concentration of unreacted ascorbic acid at nucleation resulting for differences in the time between addition of reactants. These results are also consistent with the comproportionation scheme for ascorbic acid suggested by Scarabelli *et al.*¹⁵

The observed changes in λ_{LSPR} with $[AA]$ seen here support reports elsewhere that aspect ratio increases with increasing $[AA]$ but begins to drop at higher values of $[AA]$.^{48,49} However contradictory reports exist in the literature suggesting that increasing $[AA]$ should cause a decrease in aspect ratio (i.e. refs. 50 & 51). Increasing $[AA]$ will substantially speed up the reaction and appears to have little impact on the quality of the product based on their spectra alone. This decreased synthesis time could potentially enable this method to be used in continuous flow methods, enabling syntheses to be substantially scaled up for industrial production.

3.4. Effect of sodium borohydride concentration. NaBH_4 is a strong reductant used to induce nucleation in this protocol and plays the same role as the seed solutions added during seeded monocrystalline AuNR syntheses.

To explore the effect of varying $[\text{NaBH}_4]$ this in our system, a single growth solution was prepared containing $[\text{CTAB}] = 48 \text{ mM}$, $[\text{oleate}] = 12.5 \text{ mM}$, and $[\text{Au}] = 0.5 \text{ mM}$. This was aliquoted into 10 mL batches and $[\text{NaBH}_4]$ varied between 1.9 and 15.4 μM . A clear increase in λ_{LSPR} was seen with increasing $[\text{NaBH}_4]$, indicating that higher aspect ratio AuNRs were synthesized (Figure 4(a) and (b)). λ_{LSPR} for $[\text{NaBH}_4] = 1.9 \text{ }\mu\text{M}$ did not match the trend seen for higher $[\text{NaBH}_4]$. It is unclear whether this resulted from some new particle growth regime at low $[\text{NaBH}_4]$. Given that there is expected to be an increased number of AuNRs with increasing $[\text{NaBH}_4]$, and the same finite reservoir of Au ions, it is assumed that these higher aspect-ratio AuNRs must be of reduced diameter.

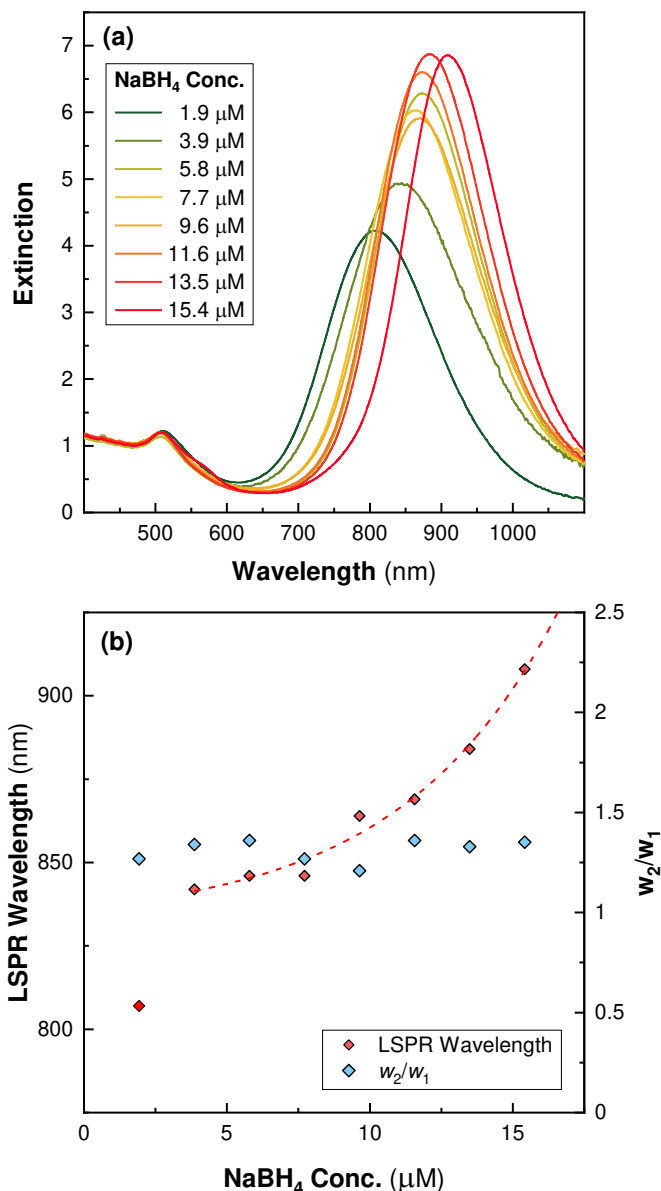


Figure 4. Effect of varying $[\text{NaBH}_4]$ on AuNR spectra ($[\text{CTAB}] = 48 \text{ mM}$, $[\text{oleate}] = 12.5 \text{ mM}$). **(a)** UV-Vis spectra normalized to $A_{400\text{nm}}$. A general trend of increasingly redshifted λ_{LSPR} values can be seen with increasing $[\text{NaBH}_4]$. Low $[\text{NaBH}_4]$ can be seen to lead to broader longitudinal surface plasmon resonance (LSPR) peaks (more polydisperse). **(b)** λ_{LSPR} as a function of $[\text{NaBH}_4]$, demonstrating the increase in λ_{LSPR} with increasing $[\text{NaBH}_4]$. The red data point associated with 2 μL is not included in the fit. Also plotted is w_2/w_1 for spectra with a longitudinal surface plasmon resonance peak well separated from the transverse peak. **[single column]**

All longitudinal surface plasmon resonance peaks had relatively low asymmetry as measured by w_2/w_1 , remaining consistently around a value of ~ 1.3 , suggesting that the polydispersity was low and $[NaBH_4]$ had little impact on the AuNR polydispersity. For all spectra near complete reduction of the Au^{3+} occurred, based on the final A_{400nm} being close to 1.2 ($[Au^0] \sim 0.5$ mM) for all spectra.

There are conflicting reports of the effect of changing $[NaBH_4]$ (or equivalently concentration of seeds) added to the growth mixture, with multiple reports that an increase leads to a blueshift in λ_{LSPR} ^{17,37,52,53} and several others observing a redshift.^{14,18,19,39,42,54} Our results match the observations of the latter group reporting a redshift. There have been some suggestions that the effect of $[NaBH_4]$ is highly dependent on the pH and relative concentrations of other components in the growth solution.^{14,17} Consistent with our observations, other protocols using oleate have observed a redshift, however, this trend seems to be reversed at higher pH.^{20,21} It is not clear which processes are driving these changes in the AuNR aspect ratio. Increasing $[NaBH_4]$ reduces the size of each particle, as there is less Au^{3+} per nucleation. However, this does not translate into a simple relationship with the particle aspect ratio.

Our results demonstrate that $[NaBH_4]$ can be used to control the aspect ratio of synthesized AuNRs, it seems that 7.5 μL is a sensible value of $[NaBH_4]$ to minimize variability between batches. $[NaBH_4] = 7.5 \mu L$ falls in a section of the curve that is less sensitive to changes in $[NaBH_4]$. The respective gradients at low (6 μL) and high (14 μL) $[NaBH_4]$ are $\sim 1 \text{ nm} \cdot \mu L^{-1}$ and $\sim 9.7 \text{ nm} \cdot \mu L^{-1}$.

3.5. Kinetic UV-Vis Spectroscopy. In our previous work, we showed that increasing the oleate concentration in this system causes a blueshift in λ_{LSPR} with an accompanying increase in length and diameter.²³ To further understand the impact of $[oleate]$ on the evolution of the AuNRs, we monitored their spectra during the synthesis. Spectra were taken at 2 min intervals and the change

in λ_{LSPR} , maximum extinction, and the full width at half-maximum (*FWHM*) of the longitudinal surface plasmon resonance peak were recorded, as well as $A_{400\text{nm}}$. From this, we can assess the concentration of reduced Au^0 in solution and approximate the average aspect ratio and monodispersity of the synthesized AuNRs.

Spectra were taken at a range of concentrations of oleate with [*CTAB*] fixed at 48 mM. The blue shifting of the longitudinal surface plasmon resonance peak with increasing [*oleate*] was observed as previously (Figures 5, S4-S7) with the same corresponding decrease in aspect ratio as observed by transmission electron microscopy (Figures S8-S12). Figure 5(a) shows the evolution of a spectrum of these samples using a growth solution with [*CTAB*] = 48 mM and [*oleate*] = 12.5 mM over 8 h. The reaction completed within ~4 h and the longitudinal surface plasmon resonance peak evolved throughout this period. Initially becoming apparent from the background after ~20 min and rapidly redshifted until around 1 h, after which it slowly blue-shifted until all Au^{3+} was exhausted (Figure 5(c)). Other researchers have reported this trend in λ_{LSPR} elsewhere.^{15,29,33,54} It suggests an initial anisotropic growth phase during which AuNR aspect ratio rapidly increases, followed by a second, more isotropic growth phase in which the aspect ratio slowly reduces.^{17,19,29}

During our experiments, there was an observable increase in $A_{400\text{nm}}$ during both phases, indicating that Au was still being reduced from the solution throughout (Figure 5(d)). This contrasts with observations by Edgar *et al.*, who using a CTAB-only synthesis (no oleate) found that the reduction in λ_{LSPR} occurred after Au^0 reduction has ceased. They thus concluded that this blueshift could not be caused by anisotropic growth, and instead must be caused by reshaping of the AuNRs themselves, primarily through modification of the end-caps from sharp crystalline facets to more rounded tip geometries.³³ However, this cannot be the case during our synthesis as

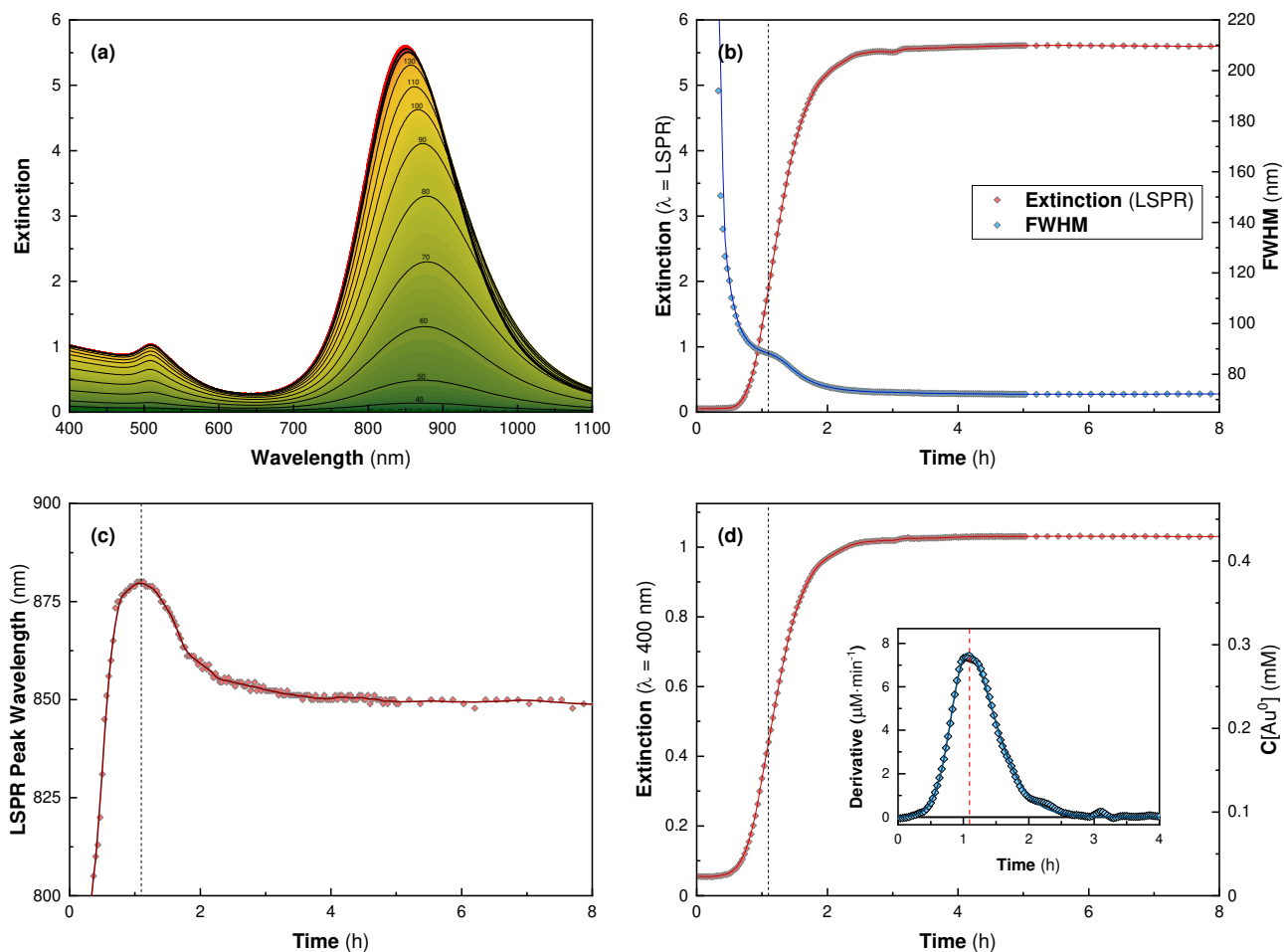


Figure 5. Kinetic UV-Vis monitoring of AuNR synthesis ($[CTAB] = 48 \text{ mM}$, $[oleate] = 12.5 \text{ mM}$). **(a)** Kinetic UV-Vis spectra of a AuNR synthesis taken at 2 min intervals. **(b)** Measured extinction at λ_{LSPR} and full width at half maximum (FWHM) of the longitudinal surface plasmon resonance (LSPR) peak as determined by a Gaussian fit. **(c)** λ_{LSPR} as a function of time, the maximum of this curve at $\sim 65 \text{ min}$ has been marked by a dashed line in (b) and (d) also. **(d)** $A_{400\text{nm}}$ (left axis) and the corresponding concentration of Au^0 calculated from $A_{400\text{nm}}$ (right axis). Inset is the derivative given in μM of Au^{1+} reduced per min. **[double column]**

the Au reduction continues throughout the observed blueshift in λ_{LSPR} . In our experiments, the longest λ_{LSPR} was typically achieved at, or just before, the point of fastest Au⁰ reduction, and Au continued to be reduced onto the particles for a significant period thereafter. (Figure 5, S4-S7). It is therefore likely that Au⁰ continued to be deposited on the AuNRs in a manner which resulted in a change in aspect ratio, driving the observed shift in λ_{LSPR} . The studies mentioned above only utilize CTAB in their growth solution, completing within 30-40 min,^{33,54} by comparison the reactions here take at least 2 h to complete, often taking significantly longer than this. Processes that drive end-cap reshaping such as oxidative etching or adatom migration are unlikely to be able to compete with the rate of Au reduction onto the AuNRs seen here. There is generally little change in λ_{LSPR} once $A_{400\text{nm}}$ saturates in most cases (except for $[\text{oleate}] = 7.5 \text{ mM}$, Figure S4), implying that at high $[\text{oleate}]$, tip morphology is largely static after the completion of Au¹⁺ reduction.

The full width at half-maximum of the longitudinal surface plasmon resonance peak decreased throughout the reaction, suggesting that the polydispersity of the AuNRs consistently dropped throughout the synthesis (Figure 5(b)). There is a noticeable point of inflection in a number of these curves that occurs ~90 min after NaBH₄ addition. It is not clear what causes this, but it seems to be largely independent of $[\text{oleate}]$. Comparing $A_{400\text{nm}}$ curves between different values of $[\text{oleate}]$ shows a clear trend of decreasing Au⁰ evolution rate with increasing $[\text{oleate}]$ (Figure 6). A possible explanation for this is the increased packing density of the surfactants on the surface of the AuNR. The incorporation of more negatively charged oleate into the positively charged CTAB bilayer increases electrostatic screening between the quaternary ammonium headgroups, increasing surfactant packing and reducing the accessibility of Au¹⁺ ions to the surface of the AuNR.

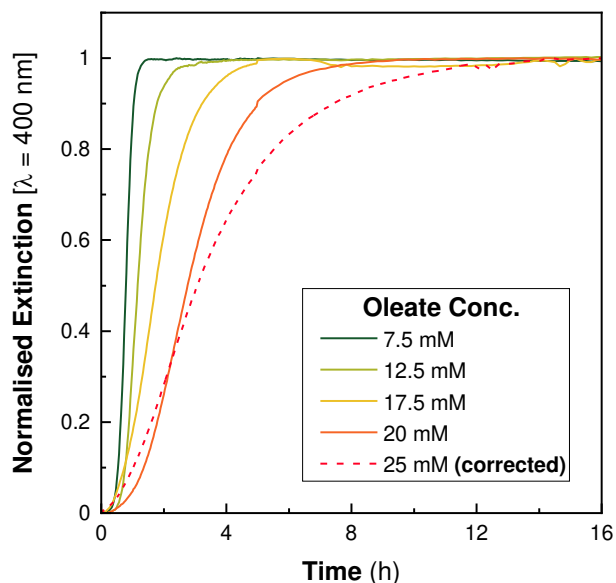


Figure 6. Effect of varying $[oleate]$ on the growth kinetics of AuNRs. Curves are normalized to the final stable value of A_{400nm} . **Note:** The $[oleate] = 25$ mM curve is not raw data, and has been corrected to account for turbidity in growth solution, see Section S2.2 for details of this.

[single column]

In our previous report, we terminated reactions after 4 h, however, the slower reaction kinetics seen here suggest that at high $[oleate]$ the reaction had not completed at this time point.²³ For instance, in the experiments reported here using $[oleate] = 20$ mM (Figure S9) resulted in A_{400nm} not increasing until ~ 6 h after $NaBH_4$ addition. This would have meant that $\sim 25\%$ of the gold precursor was wasted by separating the particles from the growth solution by centrifugation at this point. It also implies that at higher values of $[oleate]$ we erroneously concluded that these syntheses failed, when in fact a longer reaction time would have yielded useful AuNRs.

5. Conclusions.

In the CTAB-oleate AuNR synthesis, we observed dramatic changes in the optical properties of synthesized AuNRs resulting from the variation of numerous components in the growth solution.

Increasing the concentrations of HCl and Ag in the growth solutions led to redshifts of λ_{LSPR} . In the case of Ag, the optimum concentrations for growth are between ~ 80 and ~ 180 μM . Above 180 μM , particle distributions become increasingly polydisperse, with asymmetric peaks with strong tails into the near-infrared. Below 80 μM , the yield of Au^0 was reduced and the reaction kinetics slowed considerably.

Increasing the volume of NaBH_4 added to the growth solution increased the aspect ratio of synthesized particles. Similarly increasing the concentration of ascorbic acid led to an increase in aspect ratio. It also showed that oleate is doing a large proportion of the reduction of Au^{3+} to Au^0 in this synthesis. The timescale for this to complete is longer than the time between the mixing of oleate and Au and the subsequent addition of ascorbic acid. Hence, in our previous report, both oleate and ascorbic acid reduced the gold salt. For improved reproducibility, it seems that a good approach would be to allow the oleate to reduce all Au^{3+} to Au^{1+} , and the concentration of ascorbic acid adjusted accordingly.

Kinetic spectra of the binary surfactant syntheses showed that they evolve similarly to other single crystalline syntheses. The inclusion of oleate led to changes in the kinetics of the reaction. Higher oleate concentrations reduced the growth kinetics of the reaction. This meant that some reactions completed over 12 h, rather than the 2 h typically required for other syntheses. Other observations of these experiments suggest that the changes in the spectra are driven almost entirely through the direct reduction of Au onto the particles rather than via other processes causing tip reshaping. Tip reshaping is unlikely here due to there being little change in the optical spectra after gold reduction has ceased.

These observations could help with the design of future syntheses and enable the production of AuNRs with desirable optical properties. We hope that they will further assist in understanding the processes that combine to drive the formation of AuNRs during synthesis.

ASSOCIATED CONTENT

Supporting Information.

The following file is available free of charge. Additional experimental details (PDF) which contains: calibration of $[Au^0]$ from UV-Vis extinction, Effects of $[Ag]$ on reaction kinetics as measured by UV-Vis spectroscopy; Effects of $[AA]$ on reaction kinetics as measured by UV-Vis spectroscopy, Kinetic UV-Vis spectra at different $[oleate]$.

AUTHOR INFORMATION

Corresponding Author

* Stephen D. Evans, School of Physics and Astronomy, University of Leeds, Leeds, LS2 9JT, UK,
s.d.evans@leeds.ac.uk

Present Addresses

† Lucien Roach, CNRS, Univ. Bordeaux, Bordeaux INP, ICMCB, UMR 5026, 33600 Pessac, France. lucien.roach@icmcb.cnrs.fr

Author Contributions

LR performed all investigations, data curation, and formal analysis. All authors were involved in the conceptualization and design of the methodology. LR, PLC, and SDE were involved in funding acquisition. PLC, KC, and SDE administered and supervised this work. LR wrote the original draft of this manuscript. All authors were involved in the reviewing and editing of the final manuscript. All authors have approved the final version of this manuscript.

Notes

The authors declare no competing financial interest. The views expressed are those of the author(s) and not necessarily those of the NHS, the NIHR, or the Department of Health. The data associated with this paper is available from the University of Leeds: <https://doi.org/10.5518/1082>.

ACKNOWLEDGMENTS

LR would like to thank the University of Leeds for the award of a Ph.D. studentship through the University Research Scholarship. PLC expresses gratitude to the EPSRC for funding through grants EP/I000623/1, EP/P023266/1, and EP/S001069/1. KC thanks the EPSRC for financial support through grants EP/P005241/1 and EP/T013753/1. SDE would also like to thank the EPSRC for financial support (EP/P023266/1 and EP/P00122X/1). SDE is supported by the National Institute for Health Research (NIHR) infrastructure at Leeds.

ABBREVIATIONS

AA, ascorbic acid; AuNRs, gold nanorods; CTAB, cetyltrimethylammonium bromide; *FWHM*, full width at half maximum; LSPR, longitudinal surface plasmon resonance; TSPR, transverse surface plasmon resonance;

REFERENCES

- (1) Rizwan Younis, M.; He, G.; Gurram, B.; Lin, J.; Huang, P. Recent advances in gold nanorods-based cancer theranostics. *Adv. NanoBiomed Res.* **2021**, *1* (12), 2100029. [10.1002/anbr.202100029](https://doi.org/10.1002/anbr.202100029).
- (2) Huang, X.; Neretina, S.; El-Sayed, M. A. Gold nanorods: From synthesis and properties to biological and biomedical applications. *Adv. Mater.* **2009**, *21* (48), 4880. [10.1002/adma.200802789](https://doi.org/10.1002/adma.200802789).
- (3) Chen, H.; Shao, L.; Li, Q.; Wang, J. Gold nanorods and their plasmonic properties. *Chem. Soc. Rev.* **2013**, *42* (7), 2679. [10.1039/C2CS35367A](https://doi.org/10.1039/C2CS35367A).
- (4) Zheng, J.; Cheng, X.; Zhang, H.; Bai, X.; Ai, R.; Shao, L.; Wang, J.; *Chem. Rev.* **2021**, *121* (21), 13342. [10.1021/acs.chemrev.1c00422](https://doi.org/10.1021/acs.chemrev.1c00422)
- (5) Amendola, V.; Pilot, R.; Frasconi, M.; Maragò, O. M.; Iati, M. A. Surface Plasmon Resonance in Gold Nanoparticles: A Review. *J Phys Condens Matter* **2017**, *29* (20), 203002. [10.1088/1361-648X/aa60f3](https://doi.org/10.1088/1361-648X/aa60f3).
- (6) Jaque, D.; Martínez Maestro, L.; del Rosal, B.; Haro-Gonzalez, P.; Benayas, A.; Plaza, J. L.; Martín Rodríguez, E.; García Solé, J. Nanoparticles for photothermal therapies. *Nanoscale* **2014**, *6* (16), 9494. [10.1039/C4NR00708E](https://doi.org/10.1039/C4NR00708E).
- (7) Brioude, A.; Jiang, X. C.; Pileni, M. P. Optical properties of gold nanorods: DDA simulations supported by experiments. *J. Phys. Chem. B* **2005**, *109* (27), 13138. [10.1021/jp0507288](https://doi.org/10.1021/jp0507288).
- (8) Jain, P. K.; Lee, K. S.; El-Sayed, I. H.; El-Sayed, M. A. Calculated absorption and scattering properties of gold nanoparticles of different size, shape, and composition: Applications in biological imaging and biomedicine. *J. Phys. Chem. B* **2006**, *110* (14), 7238. [10.1021/jp057170o](https://doi.org/10.1021/jp057170o)
- (9) Cao, J.; Sun, T.; Grattan, K. T. V. Gold nanorod-based localized surface plasmon resonance biosensors: A review. *Sens. Actuators B* **2014**, *195*, 332. [10.1016/j.snb.2014.01.056](https://doi.org/10.1016/j.snb.2014.01.056).
- (10) Ou, Y.; Wang, X.; Lai, K.; Huang, Y.; Rasco, B. A.; Fan, Y. Gold nanorods as surface-enhanced Raman spectroscopy substrates for rapid and sensitive analysis of allura red and sunset yellow in beverages. *J Agric. Food Chem.* **2018**, *66* (11), 2954. [10.1021/acs.jafc.8b00007](https://doi.org/10.1021/acs.jafc.8b00007).
- (11) Abadeer, N. S.; Murphy, C. J. Recent progress in cancer thermal therapy using gold nanoparticles. *J. Phys. Chem. C* **2016**, *120* (9), 4691. [10.1021/acs.jpcc.5b11232](https://doi.org/10.1021/acs.jpcc.5b11232).
- (12) Jana, N. R.; Gearheart, L.; Murphy, C. J. Seed-mediated growth approach for shape-controlled synthesis of spheroidal and rod-like gold nanoparticles using a surfactant template. *Adv. Mater.* **2001**, *13* (18), 1389. [10.1002/1521-4095\(200109\)13:18<1389::AID-ADMA1389>3.0.CO;2-F](https://doi.org/10.1002/1521-4095(200109)13:18<1389::AID-ADMA1389>3.0.CO;2-F).
- (13) Nikoobakht, B.; El-Sayed, M. A. Preparation and growth mechanism of gold nanorods (NRs) using seed-mediated growth method. *Chem. Mater.* **2003**, *15* (10), 1957. [10.1021/cm020732l](https://doi.org/10.1021/cm020732l).
- (14) Ali, M. R. K.; Snyder, B.; El-Sayed, M. A. Synthesis and optical properties of small Au nanorods using a seedless growth technique. *Langmuir* **2012**, *28* (25), 9807. [10.1021/la301387p](https://doi.org/10.1021/la301387p).

- (15) Scarabelli, L.; Grzelczak, M.; Liz-Marzán, L. M. Tuning gold nanorod synthesis through prereduction with salicylic acid. *Chem. Mater.* **2013**, *25* (21), 4232. [10.1021/cm402177b](https://doi.org/10.1021/cm402177b).
- (16) Ye, X.; Jin, L.; Caglayan, H.; Chen, J.; Xing, G.; Zheng, C.; Doan-Nguyen, V.; Kang, Y.; Engheta, N.; Kagan, C. R.; Murray, C. B. Improved size-tunable synthesis of monodisperse gold nanorods through the use of aromatic additives. *ACS Nano* **2012**, *6* (3), 2804. [10.1021/nn300315j](https://doi.org/10.1021/nn300315j).
- (17) Liopo, A.; Wang, S.; Derry, P. J.; Oraevsky, A. A.; Zubarev, E. R. Seedless synthesis of gold nanorods using dopamine as a reducing agent. *RSC Adv.* **2015**, *5* (111), 91587. [10.1039/C5RA19817H](https://doi.org/10.1039/C5RA19817H).
- (18) Vigdeman, L.; Zubarev, E. R. High-yield synthesis of gold nanorods with longitudinal SPR peak greater than 1200 nm using hydroquinone as a reducing agent. *Chem. Mater.* **2013**, *25* (8), 1450. [10.1021/cm303661d](https://doi.org/10.1021/cm303661d).
- (19) Wang, W.; Li, J.; Lan, S.; Rong, L.; Liu, Y.; Sheng, Y.; Zhang, H.; Yang, B. Seedless synthesis of gold nanorods using resveratrol as a reductant. *Nanotechnology* **2016**, *27* (16), 165601. [10.1088/0957-4484/27/16/165601](https://doi.org/10.1088/0957-4484/27/16/165601).
- (20) Wadams, R. C.; Fabris, L.; Vaia, R. A.; Park, K. Time-Dependent Susceptibility of the Growth of Gold Nanorods to the Addition of a Cosurfactant. *Chem Mater* **2013**, *25* (23), 4772. [10.1021/cm402863h](https://doi.org/10.1021/cm402863h).
- (21) Ye, X.; Zheng, C.; Chen, J.; Gao, Y.; Murray, C. B. Using binary surfactant mixtures to simultaneously improve the dimensional tunability and monodispersity in the seeded growth of gold nanorods. *Nano. Lett.* **2013**, *13* (2), 765. [10.1021/nl304478h](https://doi.org/10.1021/nl304478h).
- (22) Lai, J.; Zhang, L.; Niu, W.; Qi, W.; Zhao, J.; Liu, Z.; Zhang, W.; Xu, G. One-pot synthesis of gold nanorods using binary surfactant systems with improved monodispersity, dimensional tunability and plasmon resonance scattering properties. *Nanotechnology* **2014**, *25* (12), 125601. [10.1088/0957-4484/25/12/125601](https://doi.org/10.1088/0957-4484/25/12/125601).
- (23) Roach, L.; Ye, S.; Moorcroft, S. C. T.; Critchley, K.; Coletta, P. L.; Evans, S. D. Morphological control of seedlessly-synthesized gold nanorods using binary surfactants. *Nanotechnology* **2018**, *29* (13), 135601. [10.1088/1361-6528/aaa99d](https://doi.org/10.1088/1361-6528/aaa99d).
- (24) Khlebtsov, B. N.; Khanadeev, V. A.; Ye, J.; Sukhorukov, G. B.; Khlebtsov, N. G. Overgrowth of gold nanorods by using a binary surfactant mixture. *Langmuir* **2014**, *30* (6), 1696. doi.org/10.1021/la404399n.
- (25) Pallares, R. M.; Su, X.; Lim, S. H.; Thanh, N. T. K. Fine-tuning of gold nanorod dimensions and plasmonic properties using the Hofmeister effects. *J. Mater. Chem. C* **2015**, *4* (1), 53. [10.1039/C5TC02426A](https://doi.org/10.1039/C5TC02426A).
- (26) Allen, J. M.; Xu, J.; Blahove, M.; Canonico-May, S. A.; Santaloci, T. J.; Braselton, M. E.; Stone, J. W. Synthesis of less toxic gold nanorods by using dodecylethyldimethylammonium bromide as an alternative growth-directing surfactant. *J. Colloid Interface Sci.* **2017**, *505*, 1172. [10.1016/j.jcis.2017.06.101](https://doi.org/10.1016/j.jcis.2017.06.101).
- (27) Xu, Y.; Zhao, Y.; Chen, L.; Wang, X.; Sun, J.; Wu, H.; Bao, F.; Fan, J.; Zhang, Q. Large-scale, low-cost synthesis of monodispersed gold nanorods using a gemini surfactant. *Nanoscale* **2015**, *7* (15), 6790. [10.1039/C5NR00343A](https://doi.org/10.1039/C5NR00343A).
- (28) Lohse, S. E.; Murphy, C. J. The quest for shape control: A history of gold nanorod synthesis. *Chem. Mater.* **2013**, *25* (8), 1250. [10.1021/cm303708p](https://doi.org/10.1021/cm303708p).
- (29) Walsh, M. J.; Tong, W.; Katz-Boon, H.; Mulvaney, P.; Etheridge, J.; Funston, A. M. A mechanism for symmetry breaking and shape control in single-crystal gold nanorods. *Acc. Chem. Res.* **2017**, *50* (12), 2925. [10.1021/acs.accounts.7b00313](https://doi.org/10.1021/acs.accounts.7b00313).
- (30) Tong, W.; Walsh, M. J.; Mulvaney, P.; Etheridge, J.; Funston, A. M. Control of symmetry breaking size and aspect ratio in gold nanorods: Underlying role of silver nitrate. *J. Phys. Chem. C* **2017**, *121* (6), 3549. [10.1021/acs.jpcc.6b10343](https://doi.org/10.1021/acs.jpcc.6b10343).
- (31) Liu, M.; Guyot-Sionnest, P. Mechanism of silver(I)-assisted growth of gold nanorods and bipyramids. *J. Phys. Chem. B* **2005**, *109* (47), 22192. [10.1021/jp054808n](https://doi.org/10.1021/jp054808n).

- (32) Niidome, Y.; Nakamura, Y.; Honda, K.; Akiyama, Y.; Nishioka, K.; Kawasaki, H.; Nakashima, N. Characterization of silver ions adsorbed on gold nanorods: Surface analysis by using surface-assisted laser desorption/ionization time-of-flight mass spectrometry. *Chem. Commun.* **2009**, *13*, 1754. [10.1039/B821402F](https://doi.org/10.1039/B821402F).
- (33) Edgar, J. A.; McDonagh, A. M.; Cortie, M. B. Formation of gold nanorods by a stochastic “popcorn” mechanism. *ACS Nano* **2012**, *6* (2), 1116. [10.1021/mn203586j](https://doi.org/10.1021/mn203586j).
- (34) Khan, Z.; Singh, T.; Hussain, J. I.; Hashmi, A. A. Au(III)–CTAB reduction by ascorbic acid: Preparation and characterization of gold nanoparticles. *Colloids Surf. B* **2013**, *104*, 11. [10.1016/j.colsurfb.2012.11.017](https://doi.org/10.1016/j.colsurfb.2012.11.017).
- (35) Khlebtsov, N. G. Determination of size and concentration of gold nanoparticles from extinction spectra. *Anal. Chem.* **2008**, *80* (17), 6620. [10.1021/ac800834n](https://doi.org/10.1021/ac800834n).
- (36) Shard, A. G.; Wright, L.; Minelli, C. Robust and accurate measurements of gold nanoparticle concentrations using UV-Visible spectrophotometry. *Biointerphases* **2018**, *13* (6), 061002. [10.1116/1.5054780](https://doi.org/10.1116/1.5054780).
- (37) Scarabelli, L.; Sánchez-Iglesias, A.; Pérez-Juste, J.; Liz-Marzán, L. M. A “tips and tricks” practical guide to the synthesis of gold nanorods. *J. Phys. Chem. Lett.* **2015**, *6* (21), 4270. [10.1021/acs.jpcclett.5b02123](https://doi.org/10.1021/acs.jpcclett.5b02123).
- (38) Nguyen, T. N. H.; Nguyen, T. L. T.; Luong, T. T. T.; Nguyen, C. M. T.; Nguyen, T. P. P. Synthesis of gold nanorods with a longitudinal surface plasmon resonance peak of around 1250 nm. *Adv. Nat. Sci. Nanosci. Nanotechnol.* **2016**, *7* (1), 015006. [10.1088/2043-6262/7/1/015006](https://doi.org/10.1088/2043-6262/7/1/015006).
- (39) Salavatov, N. A.; Dement’eva, O. V.; Mikhailichenko, A. I.; Rudoy, V. M. Some aspects of seedless synthesis of gold nanorods. *Colloid J.* **2018**, *80* (5), 541. [10.1134/S1061933X18050149](https://doi.org/10.1134/S1061933X18050149).
- (40) Orendorff, C. J.; Murphy, C. J. Quantitation of metal content in the silver-assisted growth of gold nanorods. *J. Phys. Chem. B* **2006**, *110* (9), 3990. [10.1021/jp0570972](https://doi.org/10.1021/jp0570972).
- (41) Smitha, S. L.; Gopchandran, K. G.; Ravindran, T. R.; Prasad, V. S. Gold nanorods with finely tunable longitudinal surface plasmon resonance as SERS Substrates. *Nanotechnology* **2011**, *22* (26), 265705. [10.1088/0957-4484/22/26/265705](https://doi.org/10.1088/0957-4484/22/26/265705).
- (42) Ye, T.; Dai, Z.; Mei, F.; Zhang, X.; Zhou, Y.; Xu, J.; Wu, W.; Xiao, X.; Jiang, C. Synthesis and optical properties of gold nanorods with controllable morphology. *J. Phys. Condens. Matter* **2016**, *28* (43), 434002. [10.1088/0953-8984/28/43/434002](https://doi.org/10.1088/0953-8984/28/43/434002).
- (43) Jéssl, S.; Tebbe, M.; Guerrini, L.; Fery, A.; Alvarez-Puebla, R. A.; Pazos-Perez, N. Silver-assisted synthesis of gold nanorods: The relation between silver additive and iodide impurities. *Small* **2018**, *14* (20), 1703879. [10.1002/sml.201703879](https://doi.org/10.1002/sml.201703879).
- (44) Theander, K.; Pugh, R. J. The influence of pH and temperature on the equilibrium and dynamic surface tension of aqueous solutions of sodium oleate. *J. Colloid Interface Sci.* **2001**, *239* (1), 209. [10.1006/jcis.2000.7543](https://doi.org/10.1006/jcis.2000.7543).
- (45) Nernst, W. Die elektromotorische Wirksamkeit der Ionen [German] (The electromotive activity of ions). *Z Phys. Chem* **1889**, *4*, 129. [10.1515/zpch-1889-0412](https://doi.org/10.1515/zpch-1889-0412).
- (46) Nernst, W. Zur Theorie der umkehrbarer galvanischer Elemente [German] (The theory of reversible Galvanic elements). *Sitzungsber. Preuss. Akad. Wiss.* **1889**, *1*, 83.
- (47) Nernst, W. Zur Kinetik der Lösung befindlichen Körper I. Theorie der Diffusion [German] (On the kinetics of bodies in solution. I. Theory of diffusion). *Z. Phys. Chem.* **1888**, *2*, 613. [10.1515/zpch-1888-0274](https://doi.org/10.1515/zpch-1888-0274).
- (48) Yoon, S.; Lee, B.; Yun, J.; Han, J. G.; Lee, J.-S.; Lee, J. H. Systematic study of interdependent relationship on gold nanorod synthesis assisted by electron microscopy image analysis. *Nanoscale* **2017**, *9* (21), 7114. [10.1039/C7NR01462G](https://doi.org/10.1039/C7NR01462G).

- (49) Miranda, O. R.; Dollahon, N. R.; Ahmadi, T. S. Critical concentrations and role of ascorbic acid (vitamin C) in the crystallization of gold nanorods within hexadecyltrimethyl ammonium bromide (CTAB)/tetraoctyl ammonium bromide (TOAB) micelles. *Cryst. Growth Des.* **2006**, *6* (12), 2747. [10.1021/cg060455l](https://doi.org/10.1021/cg060455l).
- (50) Sau, T. K.; Murphy, C. J. Seeded high yield synthesis of short Au nanorods in aqueous solution. *Langmuir* **2004**, *20* (15), 6414. [10.1021/la049463z](https://doi.org/10.1021/la049463z).
- (51) Li, P.; Wu, Y.; Li, D.; Su, X.; Luo, C.; Wang, Y.; Hu, J.; Li, G.; Jiang, H.; Zhang, W. Seed-mediated synthesis of tunable-aspect-ratio gold nanorods for near-infrared photoacoustic imaging. *Nanoscale Res. Lett.* **2018**, *13* (1), 313. [10.1186/s11671-018-2734-8](https://doi.org/10.1186/s11671-018-2734-8).
- (52) Ward, C. J.; Tronndorf, R.; Eustes, A. S.; Auad, M. L.; Davis, E. W. Seed-mediated growth of gold nanorods: Limits of length to diameter ratio control. *J. Nanomater.* **2014**, *2014*, 765618. [10.1155/2014/765618](https://doi.org/10.1155/2014/765618).
- (53) Li, M.; Zhou, R.; Liu, X.; Tao, Q. Seedless synthesis of gold nanorods by using hydrogen peroxide as a weak reducing agent. *Spectrosc. Lett.* **2019**, *52* (5), 239. [10.1080/00387010.2017.1347948](https://doi.org/10.1080/00387010.2017.1347948).
- (54) Pérez-Juste, J.; Correa-Duarte, M. A.; Liz-Marzán, L. M. Silica gels with tailored, gold nanorod-driven optical functionalities. *Appl. Surf. Sci.* **2004**, *226* (1), 137. [10.1016/j.apsusc.2003.11.013](https://doi.org/10.1016/j.apsusc.2003.11.013).